Impact of Nanostructuration on the Chemical Composition of Nickel Oxide Nanoparticles

Baptiste Polteau, François Cheviré, Franck Tessier, Philippe Deniard, Eric Gautron, Laurent Cario, Stéphane Jobic

Impact of the nanostructuration on the chemical composition of nickel oxide nanoparticles

Baptiste Polteau,[†,‡] François Cheviré,[*,†] Franck Tessier,[†] Philippe Deniard,[‡] Eric Gautron,[‡] Laurent Cario,[‡] and Stéphane Jobic[*,‡]

[†] Univ Rennes, CNRS, ISCR - UMR 6226, F-35000 Rennes, France

[‡] Institut des Matériaux Jean Rouxel, Université de Nantes, CNRS, 2 rue de la Houssinière, 44322 Nantes cedex 03, France

Supporting Information Placeholder

ABSTRACT: Reduction of the size of a particle down to a few tens of nanometer or below may drastically affect its physical properties. That is well known for quantum dots. Conversely, many works consider the chemical composition of nanoparticles as invariant when reducing their dimension. Here we demonstrate that the chemical composition of a transition metal oxide, namely nickel oxide, is drastically affected by its nanostructuration.

Nickel oxide is a well-known, strategic material that gives rise to many applications. Hence it is used in domains as diverse as solid oxide fuel cells,[1-3] lithium batteries,[4-6] electrochromic devices,[7-9] gas sensors,[10-12] (photo)catalysis,[13-15] and solar cells.[16-18] More recently, this material has been envisioned for potential memory devices due to its reversible resistance switching capability.[19-21] Finally NiO nanoparticles are also investigated for their interesting magnetic properties that are still under debate.[22-24]

NiO crystallizes in the rock salt structure. In its 1:1 stoichiometric bulky form, the material is antiferromagnetic below 523K, and exhibits a pale green color with a low electrical conductivity.[25-27] Simultaneously, NiO in the form of nanoparticles is regularly reported with different physical characteristics. Namely, a p-type semi-conductivity, a black color, or ferromagnetism are often observed.[22-24,28-32] In that context, we have embarked on the synthesis of NiO nanoparticles and their (micro)structure characterization to shed light on the impact of the nanostructuration on the Ni:O atomic ratio.

NiO materials were synthesized by thermal decomposition of $Ni_3O_2(OH)_4$ as prepared by Polteau et *al.*[33] Hereafter samples labelled NiO-T will refer as to materials prepared at the synthesis temperature T (°C). For T in the 250-500°C and 500-800°C ranges, materials exhibited a black and grey color, respectively. Above 800°C, NiO was greenish (see details in SI and **Figures S1-S2**).

Rietveld refinements were carried out on patterns collected at room temperature (RT) on each NiO-T sample. Hereafter, the "NiO" notation will stand for samples with diffraction peaks that can be fully indexed on the basis of the crystal structure of NiO even if the chemical formulae may significantly differ from the exact 1:1 atomic ratio. Refinements clearly evidenced a strong enlargement of coherent diffracting domains (i.e. CS) from 2 to 3, 4, 7, 14, 22, 32, 66 and 193nm for synthesis temperatures of 250, 300, 350, 400, 450, 500, 600, 700 and 800°C, respectively (**Figure 1** and **Table S1**). This evolution was fully asserted by transmission electron microscopy investigations (**Figures S3-S4**) that revealed well crystallized materials with a low distribution of particle size. The average particle sizes found from the examination of micrographs is almost identical to CS determined by XRD (**Table S1**). Consequently, nanoparticles can be viewed as single crystals, and not as an assembly of crystallites, *i.e.* grains.

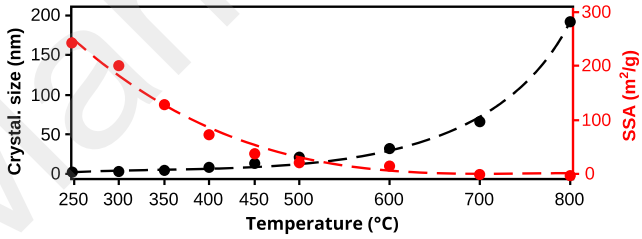

Figure 1. Crystallite size (CS) (black dots) and specific surface area (red dots) of "NiO" samples prepared from $Ni_3O_2(OH)_4$ at temperatures ranging from 250°C to 800°C.

This reduction of the nanoparticule size with increasing temperature goes along with a strong diminution of the specific surface areas (SSA) of NiO-T samples that were determined by the Brunauer-Emmett-Teller method. **Figure 1** displays the evolution of SSA *vs.* T and evidences a continuous decrease from 240m^2/g to 3m^2/g for NiO-250 and NiO-800 samples, respectively. All nanoparticles prepared from decomposition of the precursor above 200°C crystallize therefore with the rock salt structure but exhibit different particle sizes.

To get insight on the impact of the particle size on the chemical composition of the nanoparticles we have performed chemical analyses and density measurements (ρ_{exp}) on NiO-T samples. The ρ_{exp} *vs.* T curve is displayed in **Figure 2** (see also **Table S2**). Clearly, samples prepared at temperature higher than 600°C (with CS higher than 30 nm) exhibit a density quite similar to the theoretical one (ρ_{theo}=6.81 g/cm^3). At the opposite, density for samples prepared below 600°C is lower than ρ_{theo} and can reach value as low as 5.14g/cm^3 for T equal to 250°C (CS of 2.3nm). At this stage, the weight oxygen content (O wt%) of each samples was determined by the inert gas fusion method (**Figure S5 and Table S2**). Samples prepared at low temperatures clearly evidenced an oxygen concentration much higher (*e.g.* 26.8 wt% for NiO-250) than the expected one for 1:1 Ni:O stoichiometric materials (*i.e.* 21.41%). However, when synthesis temperature increases, the oxygen weight percentage tends to decrease to reach the theoretical value expected for a 1 by 1 stoichiometry. Thus, the discrepancy in the density measurements at low T can be assigned to a nickel off-stoichiometry ($Ni_{1-x}O$), the refined cell volumes re-

maining quite similar for all samples (**Table S2**). For "NiO" nanoparticles with spherical shape and hypothetical $Ni_{1-x}O$ chemical composition, the density can be written $\rho_{(exp)}=(Z\times M)/(N_A\times V_{cell})$ where Z, M, N_A and V_{cell} are the number of formula unit per unit cell, the molar mass of $Ni_{1-x}O$, the Avogadro number and the volume of the unit cell. Subsequently, the nickel deficiency in $Ni_{1-x}O$ can be calculated from the density measured experimentally and the cell volume determined by Rietveld refinement. **Figure 2** displays the calculated x value of the $Ni_{1-x}O$ samples versus T. Clearly amazing x values as high as 0.30, 0.23 and 0.18 are calculated for NiO-250, NiO-300 and NiO-350 samples. When synthesis temperatures increase, x values progressively decrease to reach more reasonable values at *ca.* 450°C, and finally tend to zero for T higher than 600°C.

Consequently, our study clearly confirms that the stoichiometry of the nanoparticle (*i.e.* the Ni:O ratio) is strongly correlated to the particle size. Two models can be envisioned to explain the origin of such high Ni vacancy rates. Either nickel vacancies are homogeneously distributed over the whole material or nickel vacancies are segregated at the surface of nanoparticles. The former hypothesis

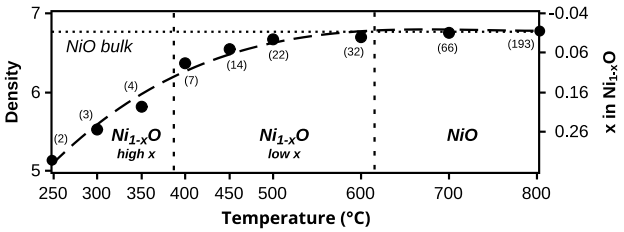

Figure 2. Evolution of the density and the Ni off-stoichiometry of NiO-T samples versus their synthesis temperature. The dashed line has to be regarded as a guide to the eyes. Calculated crystallite sizes (in nanometers) are indicated within brackets.

may be discarded as it would imply an incredible stability of the crystal structure type to accept such high concentrations of defects. Moreover, the segregation of metal vacancies at the surface of the nanoparticles was already observed for $Zn_{1-x}O$ nanoparticles synthesized by thermal decomposition of ZnO_2.[34-35] The density *vs.* particle size curve was then successfully explained by a core-shell model involving the segregation of metal vacancies at the surface. This model is extended here to NiO nanoparticles by considering a core consisting of NiO bulk (*i.e.* a stoichiometric NiO) and a shell of an oxygen rich (Ni poor) material. Under oxidizing conditions (decomposition of the $Ni_3O_2(OH)_4$ oxygen-rich precursor in air), it is reasonable to anticipate that the surface of the synthesized "NiO" samples would be likely composed of a layer of oxygen atoms or hydroxyl groups. To some extent, the shell could be viewed as a passivating layer that might contain altogether species as O^{2-}, OH^-, CO_3^{2-} or H_2O. In this core-shell model, the ratio of the top-layer thickness (e) over the total particle radius (R) will be large for a nanoparticle but will decrease when the particle grows up as detailed in **Figure S6a**. Namely, based on a simple mathematical treatment with successive iterations on the e value (Model 1, see **SI** for methodology), the thickness of the top-layer can be estimated between 1.3Å and 2.5Å depending on whether the density evolution is fitted versus the crystallite size (**Figure S6b)** or the specific surface area (**Figure S6c**). This thickness value is completely consistent with a top-layer made of a single atomic layer passivating naturally the surface of the nanoparticles and consisting of oxygen or hydroxyl species with Ni-O interatomic distances of *ca*. 1.8Å.

This core-shell model was subsequently refined starting from the rock salt structure type of NiO built upon $[NiO_6]$ octahedra sharing edges to form a tridimensional edifice. The crystal growth of NiO was then considered starting from a regular $[NiO_6]$ polyhedron as a seed. At the very first stage of the growth, this octahedron will be surrounded by 18 nickel atoms that will complete their coordination sphere via the addition of 38 oxygen atoms to be six-fold coordinated. This growth process will pursue as shown in **Figure 3a**. The particle will maintain its overall octahedral shape throughout its growth as long as oxygen atoms will cover the external surfaces. Namely, the crystal growth procedure will follow a mathematical series called octahedral number (*On*) defined as $On=n\times(2n^2+1)/3$; *On* enumerates the total quantity of Ni and O atoms within the octahedral particle for odd and even n number, respectively. Hence, the second, third, fourth, fifth and sixth coordination spheres of Ni will contain 6 O atoms (n=2, *On*=6), 18 Ni atoms (n=3, *On*=19), 38 O atoms (n=4, *On*=44), 66 Ni atoms (n=5, *On*=85), and 102 O atoms (n=6, *On*=146), etc. Consequently, at each stage of the growth process, the total number of atoms of nickel and oxygen can be determined, as well as the exact stoichiometry of the nanoparticles and their theoretical density. **Table S3** sums up for even n values (*i.e.* oxygen terminated nanoparticles) salient values, namely the number of Ni and O atoms, the deviation to the 1:1 stoichiometry, the octahedron diagonal, the particle diameter assimilated to the isovolumic sphere diameter as depicted in **Figure 3b** inset, and the calculated density. Data are given for octahedral particles with apical distances lower than 6nm (n from 2 to 14), and at *ca*. 100nm (n=242) and 400nm (n=960).

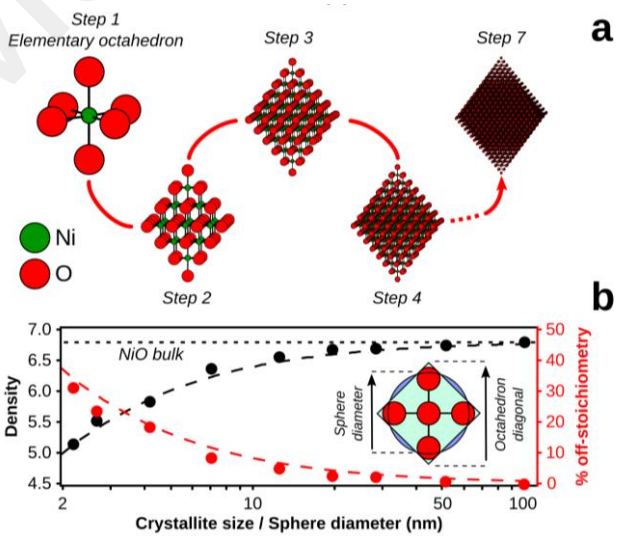

Figure 3. (a) Schematic representation of the crystal growth of NiO from a $[NiO_6]$ seed as described in the text. (b) Evolution of the measured density (black dots) and the calculated Ni off-stoichiometry (red dots) in "NiO" *vs.* crystal size, and comparison with models (dotted lines) where crystal size is assimilated to the isovolumic sphere diameter ($\varnothing_{sphere}$).

As illustrated in **Figure 3b**, a gradual increase of the density *vs.* the isovolumic sphere diameter $\varnothing_{sphere}$ is observed up to tend towards the measured bulk density of 6.81g/cm^3 for CS larger than 100nm. This goes along with a decrease of the Ni off-stoichiometry that shifts from the experimental high value of

about 30% for particles size of 2.5nm to value almost null for particles larger than 100nm (≤ 1.2%) and 400nm (0.3%). A very good correlation between theory and experiment is witnessed. This clearly proves that our core-shell model describes very well for the "NiO" nanoparticle. The core can be regarded as NiO bulk, and the shell as an oxygen single layer that naturally passivates the metallic surface. According to this model, it is possible to adjust the stoichiometry of "$Ni_{1-x}O$" materials via a fine control of the particle size.

At the nanoscale, the contribution of the surface passivation is such that it drastically modifies the chemical composition of the "NiO" particles, and potentially its physical properties. For this reason, we have measured the magnetic properties of the "NiO" nanoparticles. Many works have indeed reported the appearance of ferromagnetism in NiO nanoparticle.[36-39] **Figure 4a** displays the RT magnetization (M) of NiO-250 and NiO-800 samples *vs.* magnetic field. Nickel oxide grown at 800 °C with almost no Ni vacancies (largest particle size) exhibits no trace of ferromagnetism, which agrees with the commonly reported antiferromagnetic properties of bulk NiO. Conversely, the magnetization of the smallest nickel oxide nanoparticles (NiO-250) with a large Ni off-stoichiometry displays a clear RT ferromagnetic contribution. **Figure 4b** shows the saturation magnetization at 0.5 Tesla and RT for nanoparticles synthesized in the 250-800°C range. A clear trend is observed: the lower the particle size, the higher the ferromagnetic contribution. Our observation clearly suggests that the presence of Ni vacancies at the vicinity of the surface is at the origin of this ferromagnetic behavior. It is therefore in direct line with previous reports that also points out the prominent role of Ni vacancies in the vicinity of the surface of nanoparticles in the appearance of this ferromagnetic contribution.[36-39]

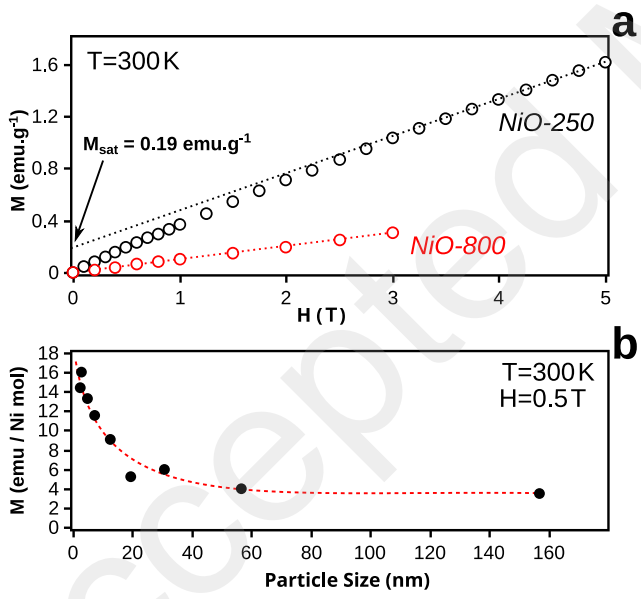

Figure 4. (a) M-H curves measured at 300K for NiO-250 and NiO-800. (b) Evolution of magnetization at 300K per Ni mol vs. particle size for NiO-T samples.

In summary, the attempts to synthesize nickel oxide via the thermal decomposition of $Ni_3O_2(OH)_4$ at low temperature leads to nanoparticles with a chemical composition exceptionally far away from the expected one (*i.e.* 1:1), with a metal deficiency up to 30%. Our work shows that besides the quantum size effect a chemical size effect has often to be taken into account to understand the behavior of transition metal oxide nanoparticles and explain the change of their physical properties with decreasing the particle size.

ASSOCIATED CONTENT

Supporting Information

The Supporting Information is available free of charge on the ACS Publications website xxxx at DOI: xxxx.
Materials preparation, characterization methods, X-ray diagrams, thermal analysis measurements, TEM photographs, density *vs.* particle size and associated tables (PDF)

AUTHOR INFORMATION

Corresponding Authors

* E-mail: francois.chevire@univ-rennes1.fr
* E-mail: stephane.jobic@cnrs-imn.fr

ACKNOWLEDGMENT

B.P. is indebted to University of Rennes and CNRS for their financial support.

REFERENCES

(1) De Souza, S.; Visco, S. J.; De Jonghe, L. C. Thin-Film Solid Oxide Fuel Cell with High Performance at Low Temperature. *Solid State Ion.* **1997**, 98, 57–6.
(2) Ricoul, F.; Subrenat, A., Joubert, O.; Le Gal La Salle, A. Electricity Production from Lignocellulosic Biomass by Direct Coupling of a Gasifier and a Nickel/Yttria-Stabilized Zirconia-Based Solid Oxide Fuel Cell. Part 1: From Gas Production to Direct Electricity Production. *Int. J. Hydrog. Energy* **2017**, 42, 21215–21225.
(3) Malzbender, J.; Wessel, E.; Steinbrech, R. W. Reduction and Re-Oxidation of Anodes for Solid Oxide Fuel Cells. *Solid State Ion.* **2005**, 176, 2201–2203.
(4) Bruce, P. G.; Scrosati, B.; Tarascon J-M. Nanomaterials for Rechargeable Lithium Batteries. *Angew. Chem. Int. Ed.* **2008**, 47, 2930–2946.
(5) Needham, S.A.; Wang, G.X.; Liu, H.K. Synthesis of NiO Nanotubes for Use as Negative Electrodes in Lithium Ion Batteries. *J. Power Sources* **2006**, 159, 254-257.
(6) Hao Liu, H.; Wang, G.; Liu, J.; Qiao, S.; Ahn, H. Highly Ordered Mesoporous NiO Anode Material for Lithium Ion Batteries with an Excellent Electrochemical Performance. *J. Mater. Chem.* **2011**, 21, 3046-3052**.**
(7) Zhang, J.; Tu, J. P.; Xia, X.H.; Qiao, Y.; Lu, Y. An All-Solid-State Electrochromic Device Based on NiO/WO_3 Complementary Structure and Solid Hybrid Polyelectrolyte. *Sol. Energy Mater. Sol. Cells* **2009**, 93, 1840–1845.
(8) Moulki, H.; Park, D. H.; Min, B-K.; Kwon, H.; Hwang, S-J.; Choy, J-H.; Toupance, T.; Campet, G.; Rougier, A. Improved Electrochromic Performances of NiO based Thin Films by Lithium Addition: From Single Layers to Devices. *Electrochim. Acta* **2012**, 74, 46–52.
(9) Granqvist; C. G. Electrochromic Devices. *J. Eur. Ceram. Soc.* **2005**, 25, 2907–2912.
(10) Dirksen, J. A.; Duval, K.; Ring, T. A. NiO Thin-Film Formaldehyde Gas Sensor. *Sens. Actuator B-Chem* **2001**, 80, 106-115.
(11) Hotovy, I.; Rehacek, V.; Siciliano, P.; Capone, S.; Spiess, L. Sensing Characteristics of NiO Thin Films as NO_2 Gas Sensor. *Thin Solid Films* **2002**, 418, 9–15.

(12) Steinebach, H.; Kannan, S.; Rieth, L.; Solzbacher, F. H_2 gas sensor performance of NiO at high temperatures in gas mixtures. *Sens. Actuators B-Chem* **2010**, 151, 162–168.
(13) Gondal, M. A.; Sayeed, M. N.; Alarfaj, A. Activity Comparison of Fe_2O_3, NiO, WO_3, TiO_2 Semiconductor Catalysts in Phenol Degradation by Laser Enhanced Photo-Catalytic Process. *Chem. Phys Lett.* **2007**, 445, 325–330.
(14) Li, L.; Duan, L., Wen, F., Li, C; Wang, M.; Hagfeldt, A.; Sun, L. Visible light Driven Hydrogen Production from a Photo-Active Cathode Based on a Molecular Catalyst and Organic Dye-Sensitized p-type Nanostructured NiO. *Chem. Commun.* **2012**, 48, 988-990.
(15) Wang, D.; Xu, R.; Wang, X.; Li, Y. NiO Nanorings and their Unexpected Catalytic Property for CO Oxidation. *Nanotechnology* **2006**, 17, 979–983.
(16) He, J.; Lindström, H.; Hagfeldt, A.; Lindquist, S-E. Dye-Sensitized Nanostructured p-type Nickel Oxide Film as a Photocathode for a Solar Cell. *J. Phys. Chem. B* **1999**, *103*, 8940–8943.
(17) Odobel, F.; Le Pleux, L.; Pellegrin, Y.; Blart, E. New Photovoltaic Devices Based on the Sensitization of p-type Semiconductors: Challenges and Opportunities. *Accounts Chem. Res.* **2010**, 43, 1063-1071.
(18) Perera, I. R.; Daeneke, T.; Makuta, S.; Yu, Z.; Tachibana, Y.; Mishra, A.; Bäuerle, P.; Ohlin, C. A.; Udo Bach, U.; Spiccia L. Application of the Tris(acetylacetonato)Iron(III)/(II) Redox Couple in p-Type Dye-Sensitized Solar Cells. *Angew. Chem. Int. Ed.* **2015**, 54, 3758-3762**.**
(19) Russo , U.; Ielmini , D.; Cagli, C.; Lacaita, A. L. Filament Conduction and Reset Mechanism in NiO-Based Resistive-Switching Memory (RRAM) Devices. *IEEE Trans. Electron Devices* **2009**, 56, 186-192.
(20) Kim, D. C.; Seo, S.; Ahn, S. E.; Suh, D.-S.; Lee, M. J.; Park, B.-H.; Yoo, I. K. ;Baek, I. G.; Kim, H.-J.;Yim, E. K.;Lee, J. E.;Park, S. O.;Kim, H. S.;Chung, U-In; Moon, J. T.; Ryu, B. I. Electrical Observations of Filamentary Conductions for the Resistive Memory Switching in NiO films. *Appl. Phys. Lett.* **2006**, 88, 202102.
(21) Lee, M-J.; Han, S.; Jeon, S. H.; Park, B. H.; Kang, B. S.; Ahn, S-E.; Kim, K. H.; Lee, C. B.; Kim, C. J.; Yoo, I-K.; Seo, D. H.; Li, X-S.; Park, J-B.; Lee, J-H., Park, Y. Electrical Manipulation of Nanofilaments in Transition-Metal Oxides for Resistance-Based Memory. *Nano Lett.* **2009**, 9, 1476-1481.
(22) Kodama, R. H.; Makhlouf, S. A.; Berkowitz, A. E. Finite Size Effects in Antiferromagnetic NiO Nanoparticles. *Phys. Rev. B.* **1997**, 79, 1393-1396.
(23) Ichiyanagi,Y.; Wakabayashi, N.; Yamazaki, J.; Yamada, S.; Kimishima, Y.; Komatsu, E.; Tajima, H. Magnetic Properties of NiO Nanoparticles. *Physica B* **2003**, 329–333, 862–863.
(24) Cooper, J. F. K.; Ionescu, A.; Langford, R. M., Ziebeck, K. R. A.; Barnes, C. H. W., Gruar, R.; Tighe, C.; Darr, J. A.; Thanh, N. T. K., Ouladdiaf, B. Core/Shell Magnetism in NiO Nanoparticles, *J. Appl. Phys.* **2013**, 114, 083906.
(25) Mott, N. F. The Basis of the Electron Theory of Metals, with Special Reference to the Transition Metals. *Proc. Phys. Soc. A* **1949**, 62**,** 416-422.
(26) Tjernberg, O.; Söderholm, S.; Karlsson, U. O.; Chiaia, G.; Qvarford, M.; Nylén, H.; Lindau, I. Resonant Photoelectron Spectroscopy on NiO. *Phys. Rev. B* **1996**, 53, 10372.
(27) Schuler, T. M.; Ederer, D. L.; Itza-Ortiz, S.; Woods, G. T.; Callcott, T. A.; Woicik, J. C. Character of the Insulating State in NiO: A Mixture of Charge-Transfer and Mott-Hubbard Character. *Phys Rev B* **2005**, 71, 115113.
(28) Gonzalez-Elipe,A. R.; Holgado, J. P.; Alvarez, R.; Munuera, G. Use of Factor Analysis and XPS To Study Defective Nickel Oxide. *J. Phys. Chem.* **1992**, 96, 3080-3086.
(29) Boschloo, G.; Hagfeldt, A. Spectroelectrochemistry of Nanostructured NiO. *J. Phys. Chem. B* **2001,** *105*, 3039-3044
(30) Korošec, R. C.; Bukovec, P. Sol-Gel Prepared NiO Thin Films for Electrochromic Applications. *Acta Chim. Slov.* **2006**, *53*, 136–147
(31) Biju, V.; Abdul Khadar, M. DC Conductivity of Consolidated Nanoparticles of NiO. *Mater. Res. Bull.* **2001**, 36, 21
(32) Madhu, G.; Biju, V. Effect of Ni^{2+} and O^{2-} Vacancies on the Electrical and Optical Properties of Nanostructured Nickel Oxide Synthesized Through a facile Chemical Route. *Physica E.* **2014**, 60, 200.
(33) Polteau, B.; Tessier, F.; Cheviré, F.; Cario, L.; Odobel, F.; Jobic, S. Synthesis of Ni-poor NiO Nanoparticles for p-DSSC Applications. *Solid State Sci.* **2016**, 54, 37-42.
(34) Renaud, A.; Cario, L.; Rocquelfelte, X.; Deniard, P.; Gautron, E.; Faulques, E.; Das, T.; Cheviré, F.; Tessier, F., Jobic, S. Unravelling the Origin of the Giant Zn Deficiency in Wurtzite Type ZnO Nanoparticles. *Sci. Rep*. **2015**, 5, 12914.
(35) Chavillon, B.; Cario, L.; Renaud, A.; Tessier, F.; Cheviré, F.; Boujtita, M.; Pellegrin, Y.; Blart, E.; Smeigh, A.; Hammarström, L.; Odobel, F.; Jobic, S. p-type Nitrogen Doped ZnO Nanoparticles Stable Over Two Years in Ambient Conditions. *J. Am. Chem. Soc.* **2012**, 134, 464-470.
(36) Mandal, S.; Banerjee, S.; Menon, K. S. R. Core-shell model of the vacancy concentration and magnetic behavior for antiferromagnetic nanoparticle. *Phys. Rev. B* **2009**, 80, 214420.
(37) Mandal, S.; Menon, K. S. R.; Mahatha, S. K.; Banerjee, S. Finite size versus surface effects on magnetic properties of antiferromagnetic particles. *Appl. Phys. Lett.* **2011**, 99, 232507.
(38) Cooper, J. F. K., Ionescu, A.; Langford, R. M.; Ziebeck, K. R. A., Barnes, C. H. W.,Gruar, R., Tighe, C.; Darr, J. A.; Thanh, N. T. K.; Ouladdiaf, B. Core/shell magnetism in NiO nanoparticles. *J. Appl. Phys.* **2013**, 114, 083906.
(39) Chen, Z-Y.; Chen, Y.; Zhang, Q. K.; Tang, X. Q.; Wang, D. D.; Chen, Z. Q.; Mascher, P.; Wang, S. J. Vacancy-Induced Ferromagnetic Behavior in Antiferromagnetic NiO Nanoparticles: A Positron Annihilation Study. *ECS J. Solid State Sci. Technol.* **2017**, 6, P798-P804.